EFFECTS OF INCLINED MAGNETIC FIELD AND SLIP BOUNDARY CONDITION ON HEAT AND MASS TRANSFER IN A CASSON NANOFLUID FLOW OVER A STRETCHING SHEET

Submited on 09/01/2020 – Accepted on 14/06/2020

Abstract

In this paper, the effects of inclined magnetic field and slip boundary condition on heat and mass transfer in a Cassonnanofluid over a stretching sheet is examined. Brownian motion and thermophoreiss with chemical reation were considered as a nanofluid model and the fluid is electrically conducting in the presence of applied an inclined magnetic field. The nonlinear partial differential equations are transformed to nonlinear ordinary differential equationsby using appropriate transformation, which is solved numerically using a spectral collocation method. The effects of some fluid parameters on velocity, temperature and nanoparticle concentration profiles are shown graphically. Enhancement of both temperature and nanoparticle concentration were observed when there is an increase in thermophoresis parameter N_t and the increase in slip parameter result to decrease in the velocity of the fluid.Local skin friction coefficient, local Nusselt number, and Sherwood number are analysed through tabulated results in table 1and 2.

Keywords: Casson nanofluid, stretching sheet, Inclined Magnetic field, Chemical reaction.

T.W AKAJE *[1]

B.I OLAJUWON [2]

Department of Mathematics, Federal University of Agriculture, Abeokuta, Nigeria.

* akajewasiu@gmail.com

INTRODUCTION

Today nanofluids are gaining more attention of many researchers because of their potential to provide enhanced performance properties, particularly with respect to heat transfer than base fluids. Choi [1] was the first author to introduce the concept of nanofluids where he proposed the suspension of nanoparticles. The suspensions of particles such as metals, metal oxides, carbides, nitrides, carbon, nanotubes etc. dispersed in base fluids such as water, ethylene glycol, refrigerants and engine oil of size less than 100nm are known as nanofluids.

Heat transfer, especially the cooling of microsystems with very large heat fluxes is the major potential application of nanofluids. This has been a focus of many researchers, where microchannel heat sinks were introduced as heat removal devices. Kandikar and Salman [2] studied the convection heat transfer in microchannels using conventional fluids like water and ethylene glycol. Provided that all systems components are carefully designed, nanofluids make a better performance for heat transfer in microchannels than base fluids. Energy loss in mechanical systems is caused majorly by friction, and this can be controlled by providing necessary lubrication to improve the efficiency of energy utilization and the reliability of mechanical systems, and this can be done by adding nanoparticles to the lubricants to enhance their tribological properties, especially in the boundary and mixed lubrication regimes.Hu et al [3] Reported, anti-friction and wear behaviours of a variety of nanoparticles used as lubricants additives, including metals and non-metals.Mustafa and Hayat [4] Discussed unsteady boundary layer flow of nano-fluid past an impulsively stretching sheet. They observed that increase in the Brownian motion and thermophoresic effect enhanced the temperature and thermal boundary layer thickness and when the strength of the thermophoresiceffefect is increase, there is enough increase in Nanoparticle concentration and rate of mass transfer at the sheet. Mathematical modelling and Computer Simulations of nanofluid flow with applications to cooling and lubrication was examined byClement and Zelin[5] and complex mixture occurred when nanoparticles are added to the base fluid (Water) at lower concentration results to physical phenomenion which have been observed in other suspensions. Analytical and numerical study of buoyancy-driven convection in a vertical enclosure filled with nanofluids has been investigated by Alloui, et al [6].investigation on convective heat transfer and flow features of nanofluids is experimentally studied by Xuan and Li [7]. The flow velocity of the fluid and the volume fraction of the nano particles increased with an increase in convective heat transfer coefficient of the nanofluid and this was bigger than that of base fluid (water) under the same velocity.Some materials display properties of the non-Newtonian fluid, which implies that they do not obey Newton's law of viscosity that's the shear stress is not linearly proportional to the rate of shear strain. Examples of such fluids are muds, tomato, glue, paint, emulsion,and condensed milk. The different models of non-Newtonian fluids base on their diverse flow behaviours have been proposed by many researchers. Casson fluid model is a preferred rheological model for many fluids including blood, honey,and sauce. When the shear stress becomes greater than the yield stress, Casson fluid starts to deform, but behave like solid when the shear stress is less than the

© Frères Mentouri University, Constantine, Algeria, 2020.

yield stress.In the category of non-Newtonian fluids, the Cassonfluid has distinct features. It has significant applications in polymer processing, industries and biomechanics.Bhattacharyya, [8] examined MHD Stagnation-Point Flow of Casson fluid and heat transfer over a stretching sheet with thermal radiation and the results show that due to thermal radiation, the temperature inside the boundary layer decreases and the velocity boundary layer thickness for Casson fluid is larger than that of a Newtonian fluid. Buoyancy and the chemical reaction effects on MHD Flow of Casson fluids through a porous medium due to a porous shrinking sheet were examined byKhalid et al[9]. The study of thermal Marangoni convection in the two-phase flow of dusty Casson fluid was investigated by Mahanthesha, and Gireesh [10]. Effects of magnetic field in squeezing flow of a Casson fluid between parallel plates analysed byNaveed et al[11] and it noticed that a strong magnetic field can be used to enhance the flow when plates are coming together and squeeze number increases the velocity profile for both the cases, i.e., when plates are coming closer and when plates are going apart.Sathies, and Gangadhar, [12] Studied the effect of chemical reaction on slip flow of MHD Casson fluid over a stretching sheet with heat and mass transfer. It is seen that in all cases the thermal boundary layer is formed and the temperature at a point decreases with, velocity ratio parameter. Analytical solution of MHD stagnation-point flow and heat transfer of Casson fluid over a stretching sheet with partial slip was presented inSamir Kumar[13]. It was noticed that the magnitude of velocity is greater in the case of Casson fluid when compared with the viscous fluid.Waqar et al [14] analysed the flow of Cassonnanofluid with viscous dissipation and convective conditions: A mathematical model. And it was found that a higher value of Casson parameter leads to a decrease in the temperature and nanoparticle concentration while effects of thermophoresis and Brownian motion parameters on nanoparticle concentration are quite opposite. Convective heat transfer and MHD effects on Cassonnanofluid flow over a shrinking sheet investigated byHussain et al[15] and the result show that the temperature profile and concentration profile decreases when both and increases.Rizwan et al[16] Investigated unsteady Cassonnanofluid flow over a stretching sheet with thermal radiation, convective and slip boundary conditions, and the study showed that by increasing the Casson, Dufour,and unsteadiness parameters, reduced the fluid velocity, temperature,and concentration profiles. Oyelakin et al[17] presented Unsteady MHD non-Darcian flow of a Cassonnanofluid between two parallel plates with heat and mass transfer and it was reported that the velocity, temperature and nanoparticles concentration is found to increase monotonously with time and that the velocity reaches the steady-state faster than the temperature and nanoparticles concentration. MHD slip flow and heat transfer of Cassonnanofluid over an exponentially stretching permeable sheet were studied by [18] and it was reported that momentum boundary layer thickness decreased with the increasing magnetic field intensity, also magnetic parameter reduced the skin friction coefficient, heat flux,andmass flux coefficients. [19] Analysed the effect of MHD and porosity on exact solutions and flow of hybrid Cassonnanofluid.

2. MATHEMATICAL FORMULATIONS

Consider the steady two-dimensionalincompressible flow of an electrically conducting and chemically reactive Cassonnanofluid bounded by a stretching sheet at $y = 0$, with the flow being confined in $y > 0. u_w = bx$ is the stretched linear velocity where b is the positive constant. Strength of the inclined magnetic field is B_o, and here $T_\infty and\ C_\infty$ are the ambient temperature and nanoparticle concentration fields with $T_\infty > T_w$. Thermophoresis and Brownian motion of nanoparticles are taken into consideration. The rheological equation of state of an isotropic and incompressible flow of Casson fluid is given by [8]:

$$\tau_{ij} = \begin{cases} \left(\mu_B + \frac{p_y}{\sqrt{2\pi}}\right) 2e_{ij}, & \pi > \pi_c \\ \left(\mu_B + \frac{p_y}{\sqrt{2\pi_c}}\right) 2e_{ij}, & \pi < \pi_c \end{cases} \quad (1)$$

where μ_D is the plastic dynamic viscosity of the non-Newtonian fluid, p_y is the yield stress of fluid, π is the product of the component of deformation rate with itself, namely, $\pi = e_{ij}e_{ij}, e_{ij}$ is the $(i,j)^{th}$component of the deformation rate and πc is the critical value of π based onthe non-Newtonian model.The governing equations of momentum, energy and mass are:

$$\frac{\partial u}{\partial x} + \frac{\partial v}{\partial y} = 0 \quad (2)$$

$$u\frac{\partial u}{\partial x} + v\frac{\partial u}{\partial y} = v\left(1 + \frac{1}{\beta}\right)\frac{\partial^2 u}{\partial y^2} - \frac{\sigma B_o^2}{\rho}\, u \sin^2 \varphi \quad (3)$$

$$u\frac{\partial T}{\partial x} + v\frac{\partial T}{\partial y} = \frac{k}{\rho_{c_p}}\frac{\partial^2 T}{\partial y^2} + \tau\left[D_B\left(\frac{\partial C}{\partial y}\frac{\partial T}{\partial y}\right) + \frac{D_T}{T_\infty}\left(\frac{\partial T}{\partial y}\right)^2\right] + \frac{\mu}{\rho_{c_p}}\left(1 + \frac{1}{\beta}\right)\left(\frac{\partial u}{\partial y}\right)^2 + \frac{\sigma B_o^2}{\rho}u^2 \sin^2 \varphi + \frac{Q_0(T - T_\infty)}{\rho_{C_p}} \quad (4)$$

$$u\frac{\partial C}{\partial x} + v\frac{\partial C}{\partial y} = D_B\frac{\partial^2 C}{\partial y^2} + \frac{D_T}{T_\infty}\frac{\partial^2 T}{\partial y^2} - K_o(C - C_\infty) \quad (5)$$

With the given boundary conditions:

$$u = u_w + \left(1 + \frac{1}{\beta}\right) N\, \rho v \frac{\partial u}{\partial y},$$

$$v = 0, T = T_w + K_1\frac{\partial T}{\partial y},\ C = C_w + K_2\frac{\partial C}{\partial y},\ at\ y = 0,$$
$$u = 0,\ T = T_\infty,\ C = C_\infty, as\ y \to \infty \quad (6)$$

where u and v are the velocity components in x and y directions respectively, u_x is the linear velocity,$\upsilon$is the kinematic fluid viscosity, ρ is the fluid density, $\beta = \mu_B\sqrt{\frac{2\pi_c}{p_y}}$ is the Cassonparameter,σ is the electrical conductivity of the fluid, T is the temperature, k is the thermal conductivity,c_p is the specific heat,T_w is the constant temperature at the sheet and T_∞ is the free stream temperature assumed to be constant,$\alpha = \frac{K}{\rho_{cp}}$I s the thermal diffusivity of the base fluid, $\tau = \frac{(\rho c)_p}{(\rho c)_f}$ is the ratio of nanoparticle heat capacity and the base fluid heat capacity, $D_B$is the coefficient of Brownian diffusion, D_T is the coefficient of thermophoretic diffusion, andB_o is the strength of the inclined magnetic field, with the induced magnetic field being neglected.

Consider the following dimensionless transformations

$$\eta = \left(\frac{b}{\upsilon}\right)^{\frac{1}{2}},\ \psi(x,y) = (b\upsilon)^{1/2}\, xf(\eta),\ \theta(\eta) = \frac{T-T_\infty}{T_w-T_\infty}, \phi(\eta) = \frac{C-C_\infty}{C_w-C_\infty} \quad (7)$$

Using the stream function $\psi(x,y)$ such that

$$u = \frac{\partial\psi}{\partial y},\ v = -\frac{\partial\psi}{\partial x} \quad (8)$$

Therefore, the equation (2) is satisfied.

From the given transformations mentioned above, 3 to 6 become

$$\left(1+\frac{1}{\beta}\right)f'''(\eta) + f(\eta)f''^{(\eta)} - \left(f'(\eta)\right)^2 - H_a\sin^2\varphi\, f'(\eta) = 0 \quad (9)$$

$$\frac{1}{Pr}\theta''(\eta) + f\theta' + N_b\phi'\theta' + N_t\theta'^2 + \left(1+\frac{1}{\beta}\right)E_c f''^2 + H_a E_c\sin^2\varphi = 0 \quad (10)$$

$$\phi'' + \mathrm{Le} f\phi' + \frac{N_t}{N_b}\theta'' - Le\chi\phi = 0 \quad (11)$$

$$f(0) = 0,\qquad f'(0) = 1 + \lambda\left(1+\frac{1}{\beta}\right)E_c f''(0),$$
$$\theta(0) = 1 + \gamma\theta'(0),\quad \phi(0) = 1 + \delta\phi'(0)$$
$$f'(\infty) = 0,\ \theta(\infty) = 0,\ \phi(\infty) = 0. \quad (12)$$

Where prime represents differentiation with respect to η, θ is the dimensionless temperature, ϕ is the dimensionless nanoparticle volume fraction, $H_a$is Hartmann number (magnetic parameter), γ is the thermal slip parameter, Le is Lewis number, χ is the chemical reaction parameter, P_r is Prandtl number, λ is the slip parameter, Ec is the Eckert number, δ is the concentration slip parameter, where N_b and N_t represent Brownian motion and thermophoresis parameters respectively.

These are defined as below:

$$Pr = \frac{v}{\alpha},\qquad Le = \frac{v}{D_B},\qquad \lambda = N\rho(vb)^{\frac{1}{2}},$$
$$\gamma = K_1\left(\frac{b}{v}\right)^{\frac{1}{2}},\qquad \chi = \frac{K_o}{b},$$
$$E_c = \frac{u^2{}_w}{c_p(T_w - T_\infty)},\qquad \delta = K_2\left(\frac{b}{v}\right)^{\frac{1}{2}},$$
$$N_b = \frac{(\rho c)_p D_B(C_w - C_\infty)}{(\rho c)_f v},$$
$$N_t = \frac{(\rho c)_p D_T(T_w - T_\infty)}{(\rho c)_f v T_\infty},\quad H_a = \frac{\sigma {B_o}^2}{\rho b},$$
$$Q = \frac{Q_0}{C\rho_{C_p}} \quad (13)$$

The physical quantities of engineering interest are the Skin friction coefficient (rate of shear stress), the Nusselt number (rate of heat transfer), and the Sherwood number (rate of mass transfer).

The local Skin-friction C_{fx}, local Nusselt Number Nu_x,and local Sherwood Number Sh_x which are defined as

$$C_{fx} = \frac{\tau_w}{\rho u^2{}_w},\qquad Nu_x = \frac{xq_w}{k(T_w - T_\infty)},$$
$$Sh_x = \frac{xq_m}{D_B(C_w - C_\infty)} \quad (14)$$

Where $\tau_w$is the shear stress, $q_w\ and\ q_m$ are the surface heat and mass flux which are given by the following expressions:

$$\tau_w = \left(\mu_B + \frac{p_y}{\sqrt{2\pi_c}}\right)\left(\frac{\partial u}{\partial y}\right)_{y=0}, q_w = -k\left(\frac{\partial T}{\partial y}\right)_{y=0}, q_m = -D_B\left(\frac{\partial C}{\partial y}\right)_{y=0} \quad (15)$$

In terms of dimensionless quantities (14) we have

$$Re_x{}^{1/2}C_f = \left(1 + \frac{1}{\beta}\right)f''(0), \quad \frac{N_u}{Re_x{}^{1/2}} = -\theta'(0), \quad \frac{Sh_x}{Re_x{}^{1/2}} = -\phi'(0), \quad (16)$$

where$Re_x = \frac{xu_w}{v}$ is the local Reynolds number.

3. METHOD OF SOLUTION

The systems of nonlinear differential equations (9-11) parallel to the boundary conditions (12) are solved numerically using the Chebyshevspectralcollocation method. In this method, the unknown functions, $f(\eta), \theta(\eta) and\ \phi(\eta)$ is approximated by the sum of the basic functions $T_n(\eta)$ [20-21]:

$$f(\eta) = \sum_{n=o}^{N} a_n T_n(\eta) \quad (17)$$

$$\theta(\xi) = \sum_{n=0}^{N} b_n T_n(\eta) \quad (18)$$

$$\phi(\eta) = \sum_{n=0}^{N} c_n T_n(\eta) \quad (19)$$

The basis functions are taken as the Chebyshev polynomials, in (17), (18) and (19) which defined in the interval $-1 \le \eta \le 1$ as

$$T_n(\eta) = \cos(N \cos^{-1}\eta) \quad (20)$$

$a_n, b_n and\ c_n$are unknown constant to be obtained. $[o, \infty]$is the considered flow problem domain, which transformed into the $[-1,1]$ of the definition of basis functions, by using the below transformation

$$\eta = \frac{2p}{p_\infty - 1} \quad (21)$$

whereη_∞ denotes the edge of the boundary layer, by substituting (17), (18) and (19) into (9-11), non-zero residual were obtained. The coefficienta_n,$b_n$andc_n were chosen in such a way that the obtained residues minimized throughout the domain.

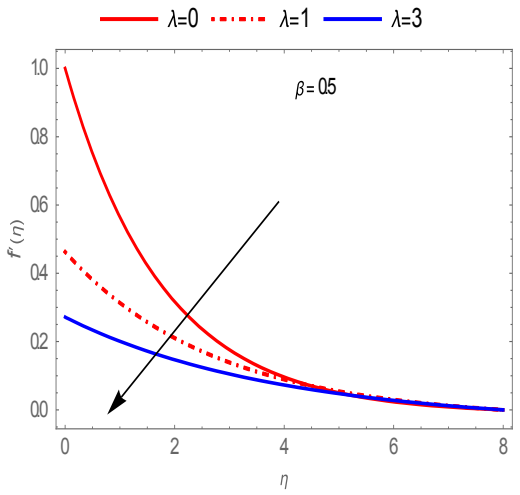

Fig. 1.Behaviour of $\lambda\ on\ f'(\eta)\ for\ \beta = 0.5$

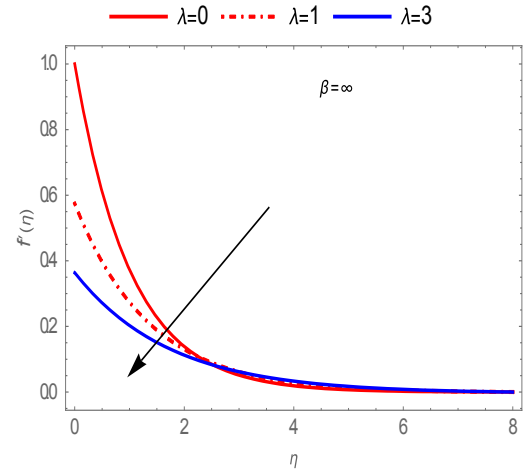

Fig. 2.Behaviour of $\lambda\ on\ f'(\eta)\ for\ \beta = \infty$

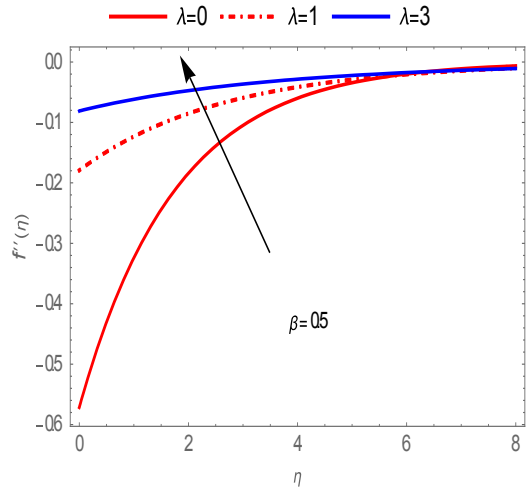

Fig. 3.Behaviour of $\lambda\ on\ f''(\eta)\ for\ \beta = 0.5$

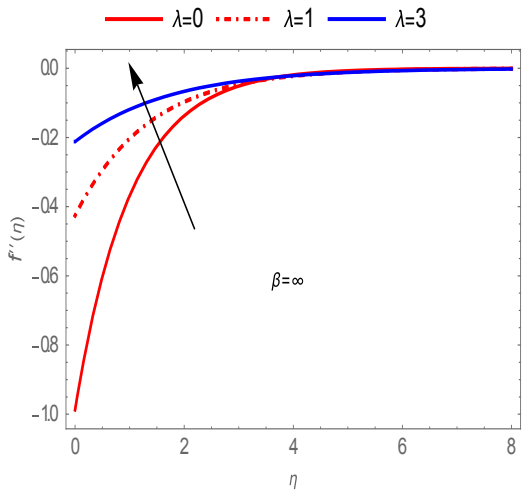

Fig. 4. Behaviour of $\lambda\ on\ f'(\eta)\ for\ \beta = \infty$

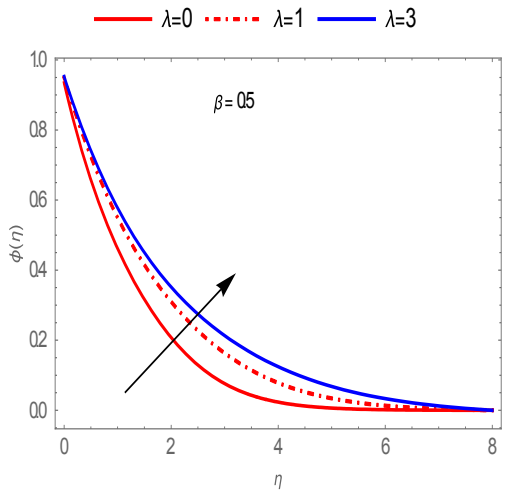

Fig. 7.Behaviour of $\lambda\ on\ \phi(\eta)\ for\ \beta = 0.5$

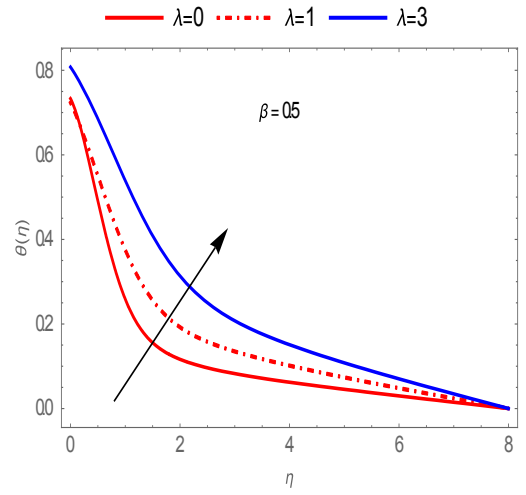

Fig. 5.Behaviour of $\lambda\ on\ \theta(\eta)\ for\ \beta = 0.5$

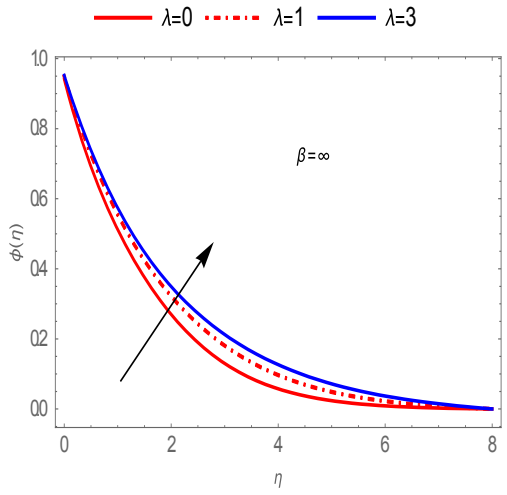

Fig. 8. Behaviour of $\lambda\ on\ \phi(\eta)\ for\ \beta = \infty$

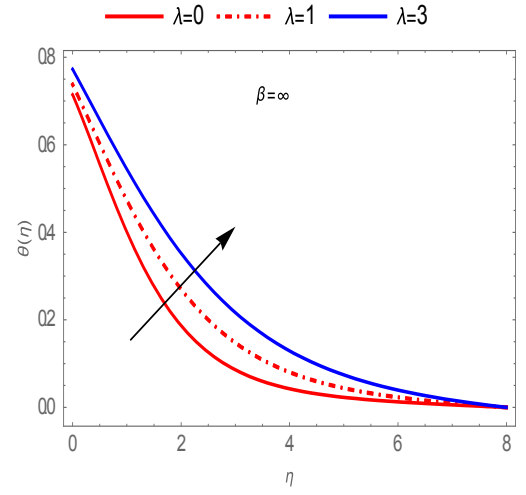

Fig. 6.Behaviour of $\lambda\ on\ \theta(\eta)\ for\ \beta = \infty$

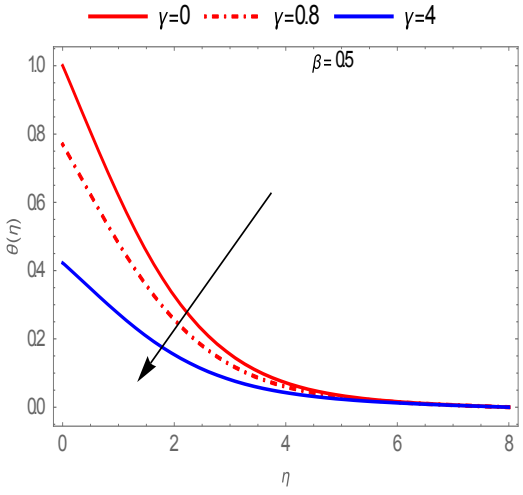

Fig. 9.Behaviour of $\gamma\ on\ \theta(\eta)\ for\ \beta = 0.5$

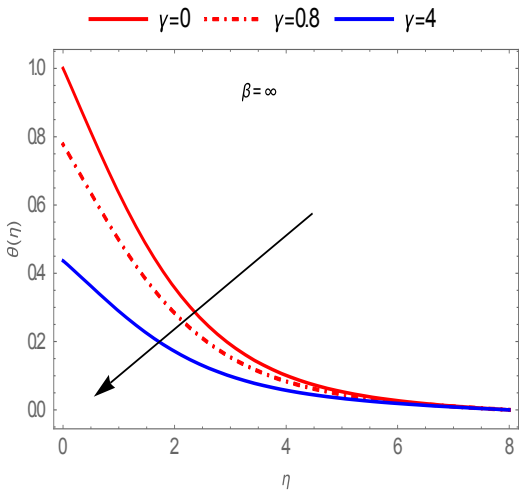

Fig. 10.Behaviour of $\gamma\ on\ \theta(\eta)\ for\ \beta = \infty$

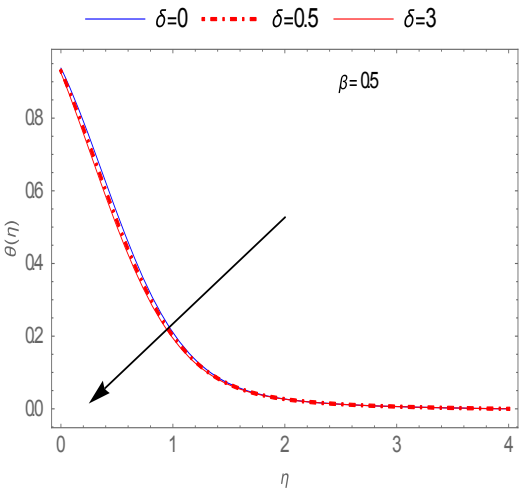

Fig. 13.Behaviour of $\delta\ on\ \theta(\eta)\ for\ \beta = 0.5,$

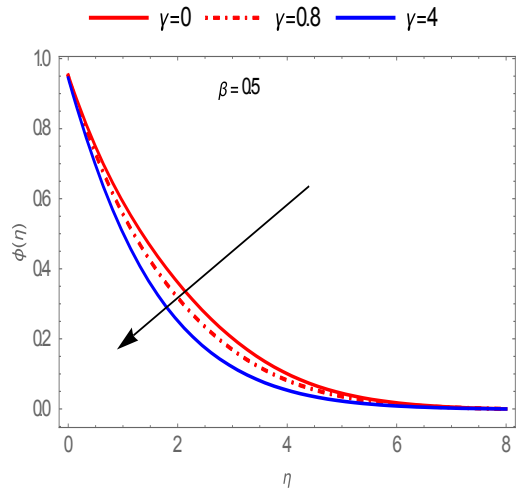

Fig. 11.Behaviour of $\gamma\ on\ \phi(\eta)\ for\ \beta = 0.5$

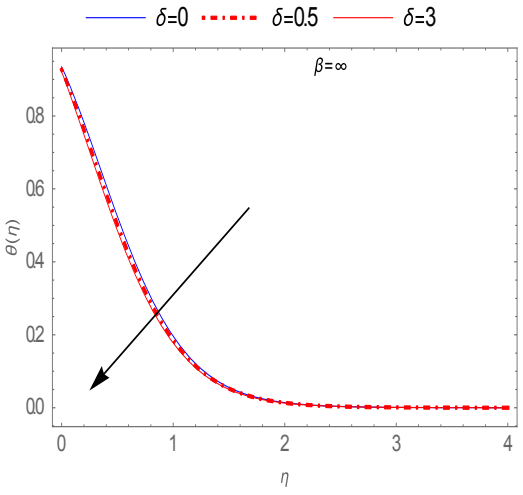

Fig. 14. Behaviour of $\delta\ on\ \theta(\eta)\ for\ \beta = \infty$

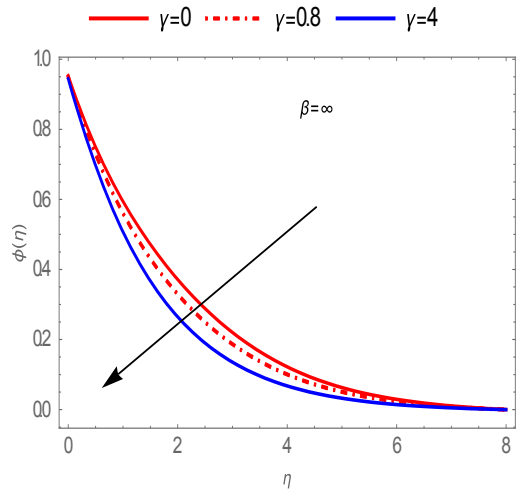

Fig. 12. Behaviour of $\gamma\ on\ \phi(\eta)\ for\ \beta = \infty$

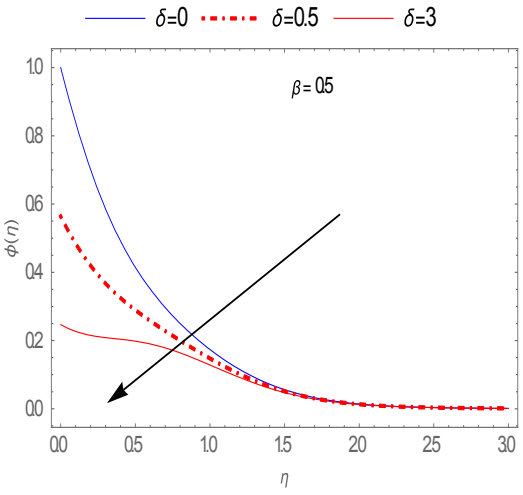

Fig.15. Behaviour of $\delta\ on\ \phi(\eta)\ for\ \beta = 0.5$

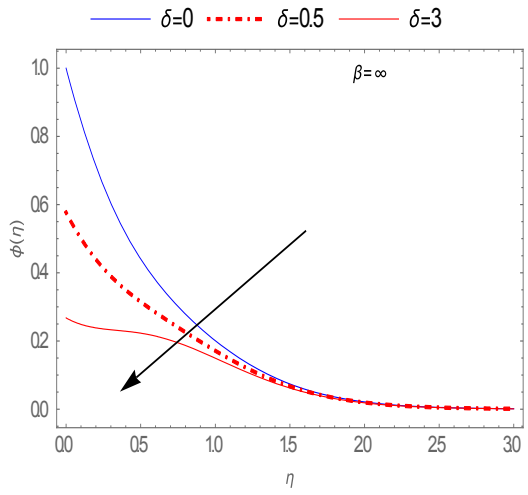

Fig. 16.Behaviour of δ on$\phi(\eta)$ for $\beta = \infty$

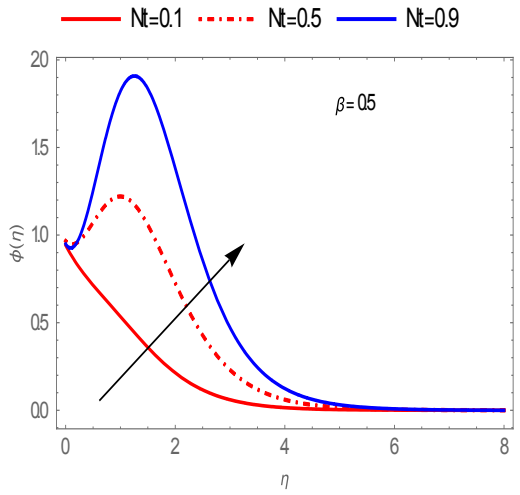

Fig. 19.Behaviour of N_t on $\phi(\eta)$ for $\beta = 0.5$

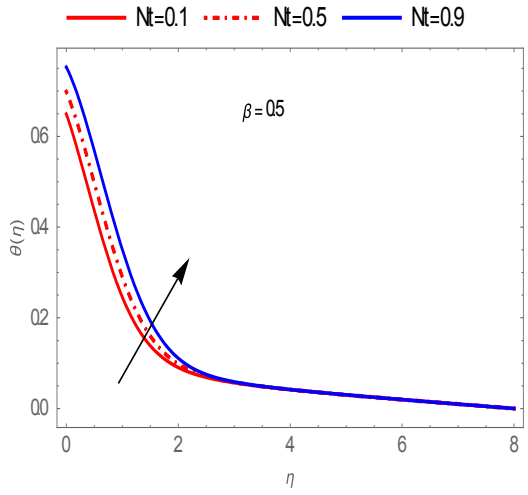

Fig.17.Behaviour of N_t on $\theta(\eta)$ for $\beta = 0.5$

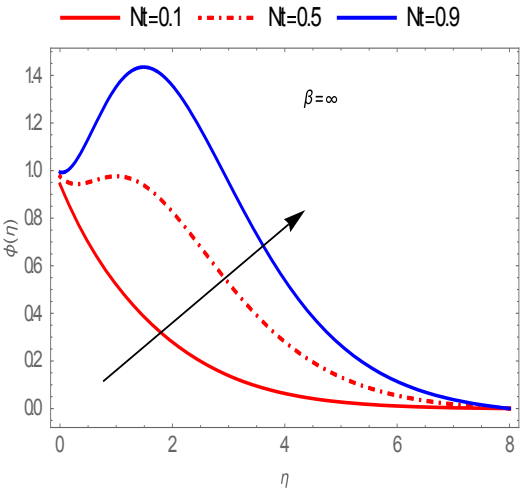

Fig. 20. Behaviour of N_t on $\phi(\eta)$ for $\beta = \infty$

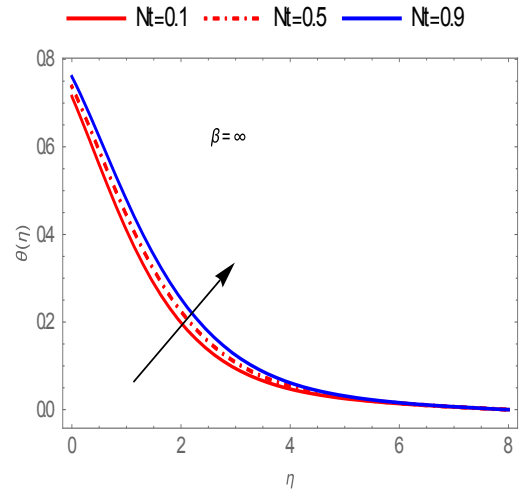

Fig. 18. Behaviour ofN_t on $\theta(\eta)$ for $\beta = \infty$

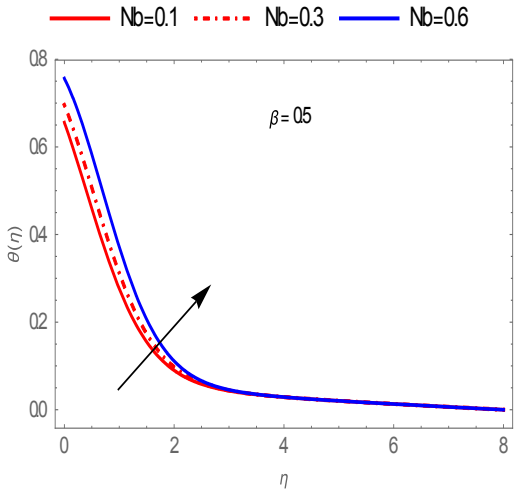

Fig. 21.Bhaviour of N_b on $\theta(\eta)$ for $\beta = 0.5$

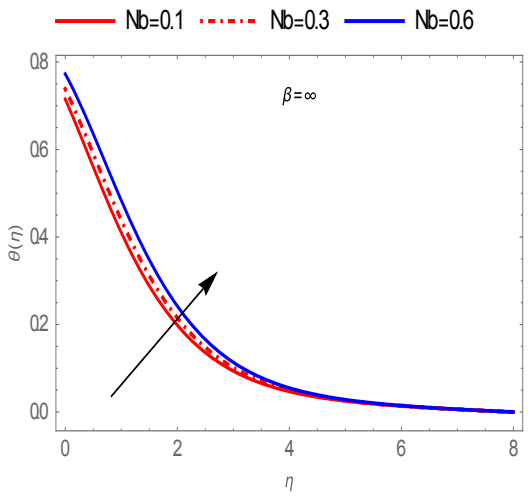

Fig. 22. Behaviour of N_b on $\theta(\eta)$ for $\beta = \infty$

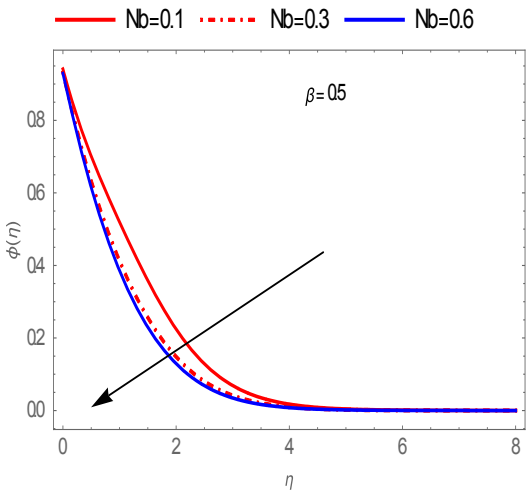

Fig.23.Behaviour of N_b on $\phi(\eta)$ for $\beta = 0.5$

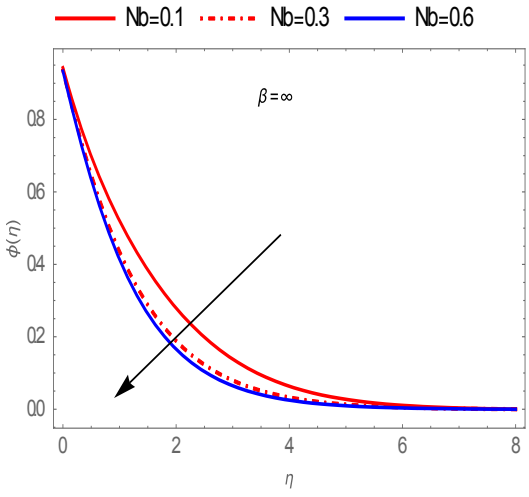

Fig.24. Behaviour of N_b on $\phi(\eta)$ for $\beta = \infty$

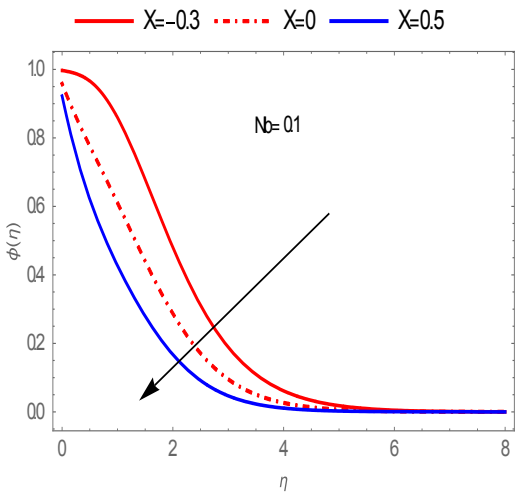

Fig. 25.Behaviour of X on $\phi(\eta)$ for $Nb = 0.1$

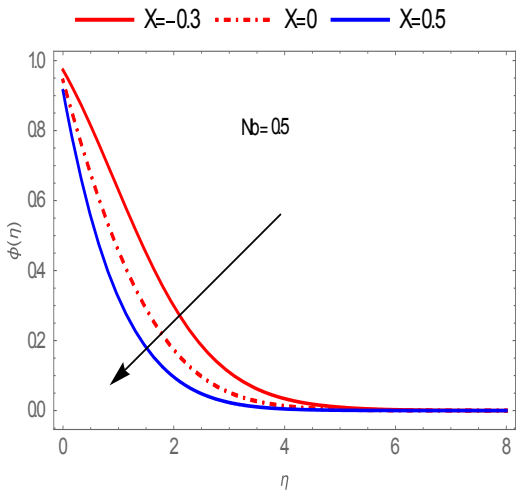

Fig. 26.Behaviour of X on $\phi(\eta)$ for $Nb = 0.5$

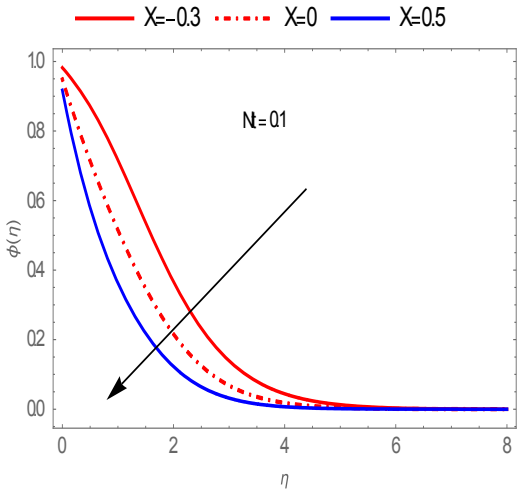

Fig. 27.Behaviour of X on $\phi(\eta)$ for $N_t = 0.1$

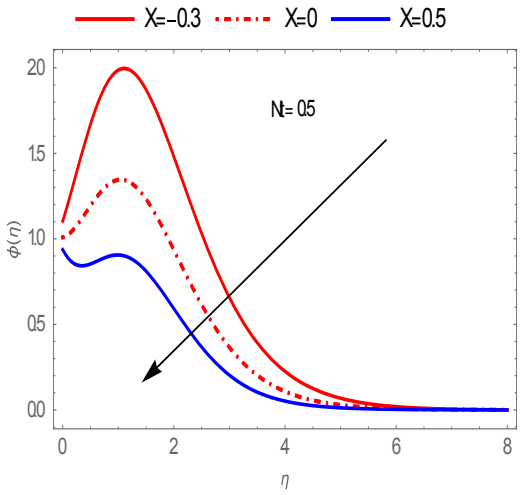

Fig. 28. Behaviour of X on $\phi(\eta)$ for $N_t = 0.5$

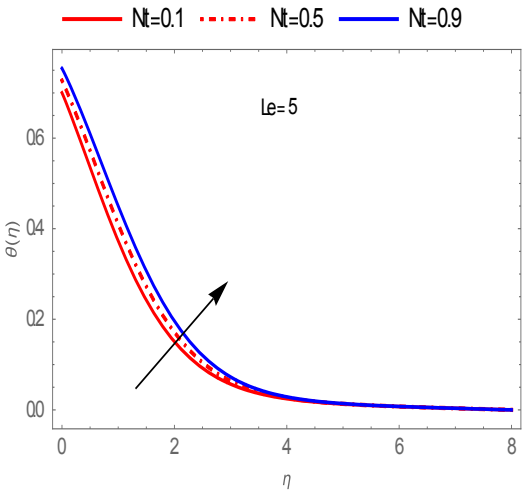

Fig. 31.Behaviour ofN_t on $\theta(\eta)$ for $Le = 5$

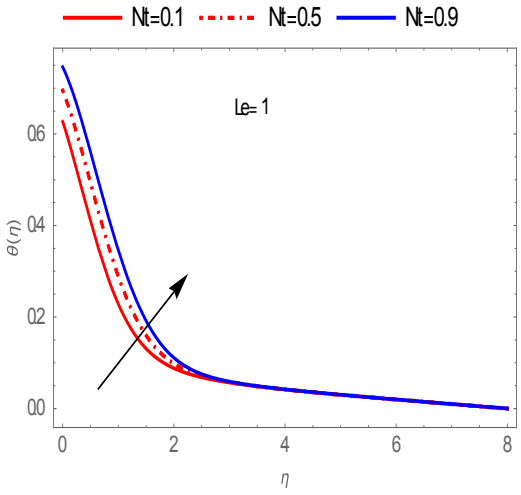

Fig. 29.Behaviour of N_t on $\theta(\eta)$ for $Le = 1$

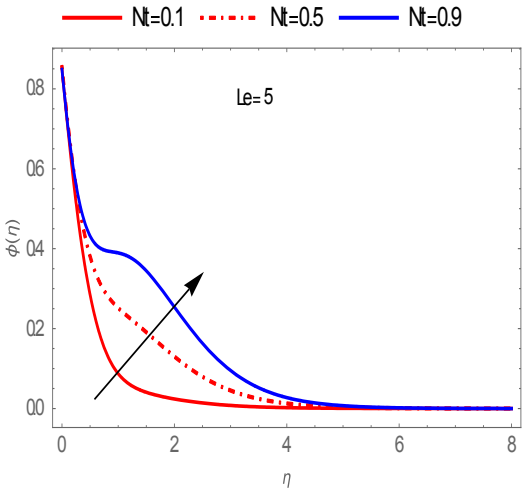

Fig. 32. Behaviour of N_t on $\phi(\eta)$ for $Le = 5$

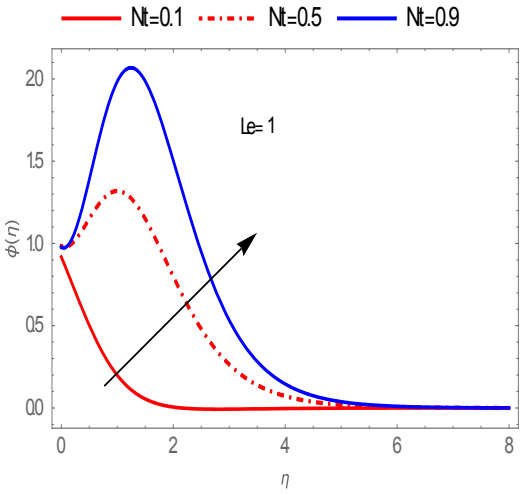

Fig. 30.Behaviour of N_t on $\phi(\eta)$ $Le = 1$

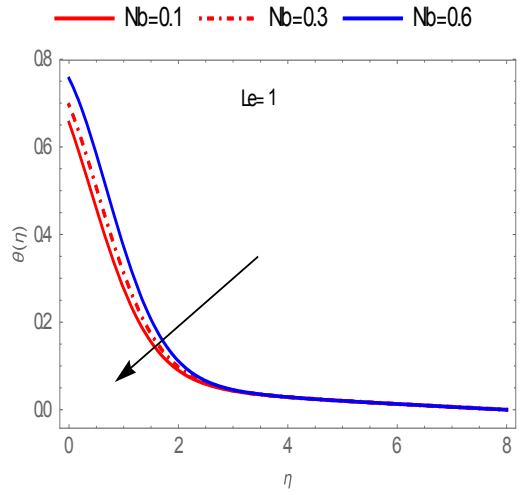

Fig. 33.Behaviour of N_b on $\theta(\eta)$ for $Le = 1$

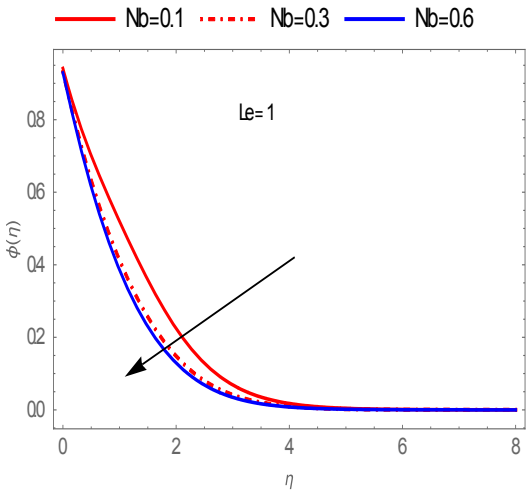

Fig. 34. Behaviour of N_b *on* $\phi(\eta)$ *for* $Le = 1$

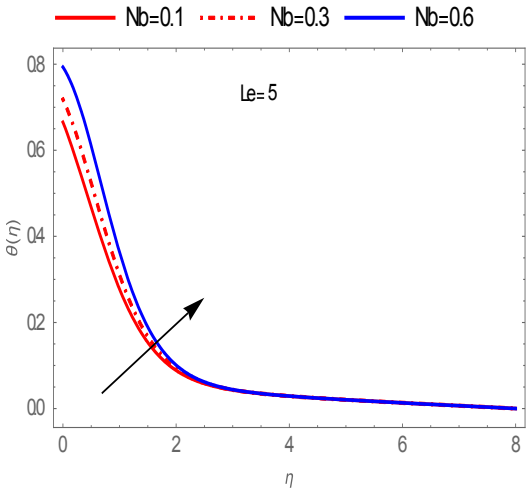

Fig. 35.Behaviour of N_b *on* $\theta(\eta)$ *for* $Le = 5$

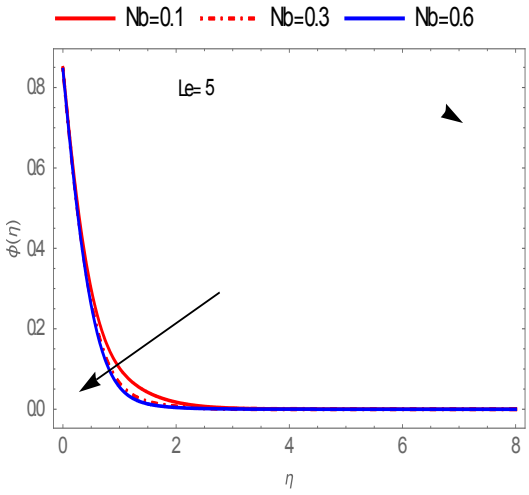

Fig. 36. Behaviour of N_b *on* $\phi(\eta)$ *for* $Le = 5$

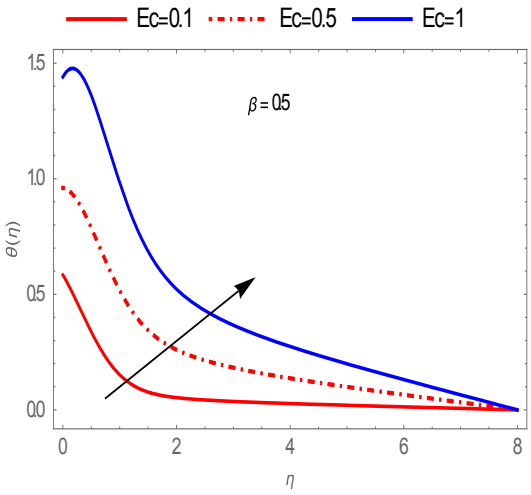

Fig. 37.Behaviour of E_c *on* $\theta(\eta)$ *for* $\beta = 0.5$

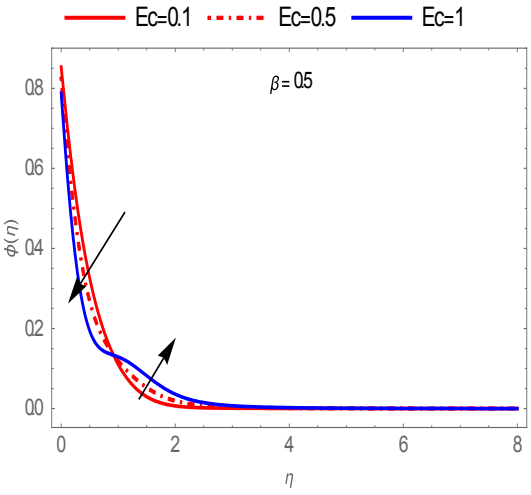

Fig. 38.Behaviour of E_c *on* $\phi(\eta)$ *for* $\beta = 0.5$

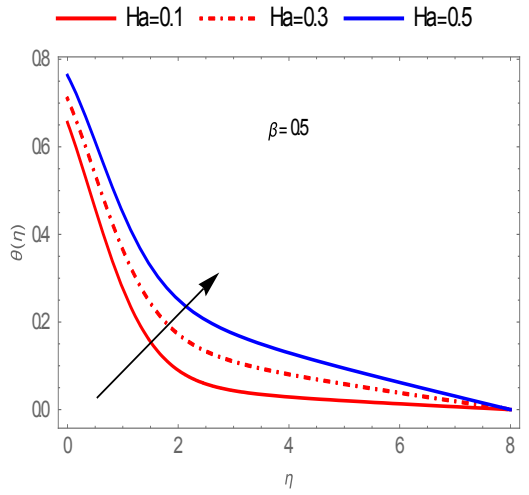

Fig.39.Behaviour of H_a *on* $\theta(\eta)$ *for* $\beta = 0.5$

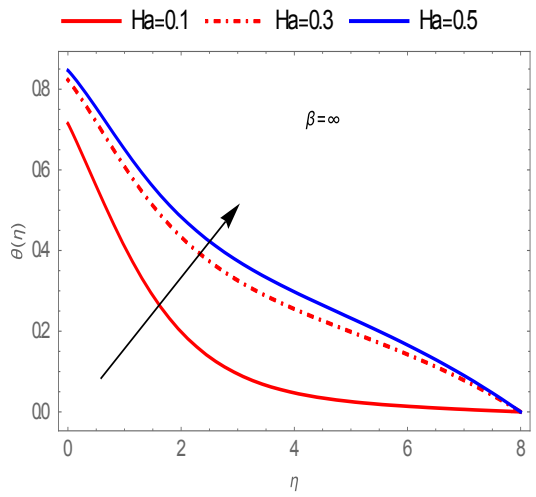

Fig. 40.Behaviour of E_a on $\phi(\eta)$ for $\beta = \infty$

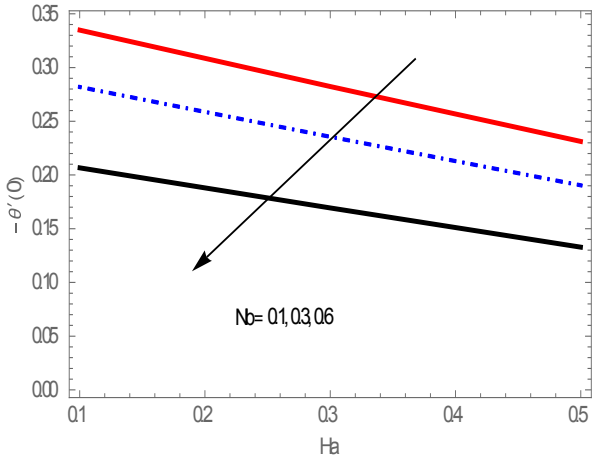

Fig. 41.Behaviour of N_b and H_a on $-\theta'(0)$

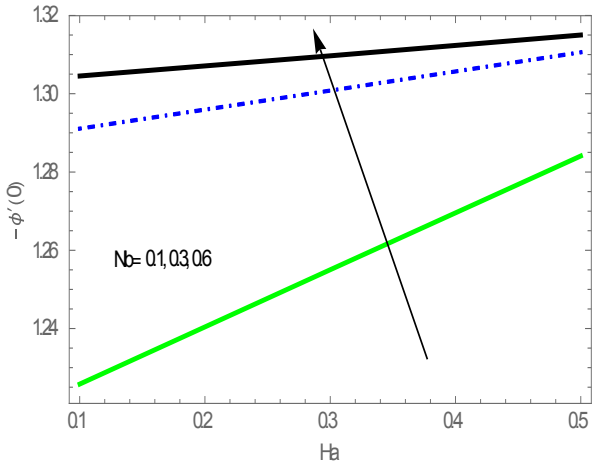

Fig. 42.Behaviour of N_b and H_a on $-\phi'(0)$

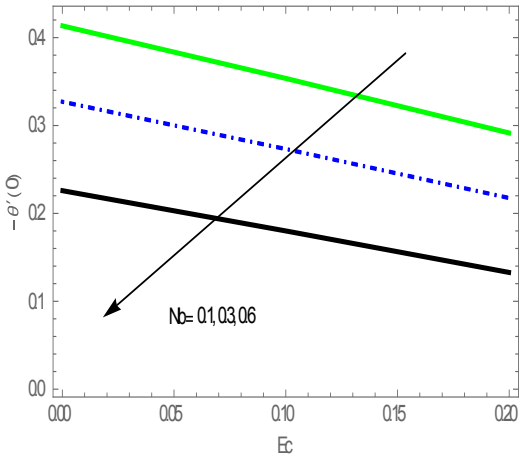

Fig. 43.Behaviour of N_b and E_c on $\theta'(0)$

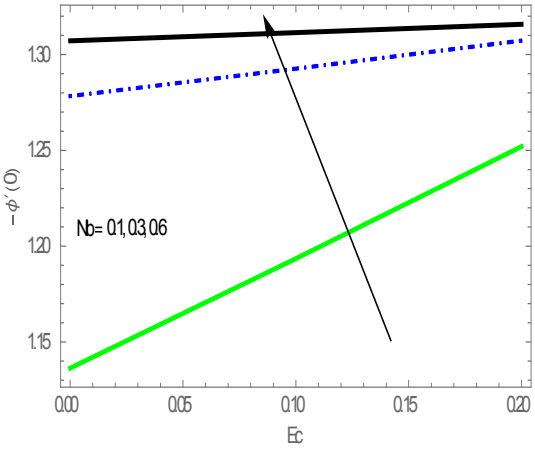

Fig. 44.Behaviour of N_b and Ec on $\phi'(0)$

4. RESULTS ANALYSIS AND DISCUSSION

The nonlinear ordinary differential equations (9) – (11) subjected to the boundary conditions in equations (12) were solved numerically using Spectral collocation Method. The obtained results are displayed through graphs figures 2-35for dimensionlessvelocity, dimensionlesstemperature and dimensionless Nanoparticle concentration profiles were studied, as well as the skin friction coefficient, local Nusselt and Sherwood numbers.

Figs. 1-4 are plotted to examine the influence of slip parameter on both velocity profile and the magnitude of the Skin friction coefficient, it was observed that an increase in slip parameter reduced the velocity of the fluid flow and the magnitude of the Skin friction coefficient increased. Figs. 5-8 illustrate the effect of slip parameter on temperature and nanoparticle concentration profiles and it was shown graphically that an increase in slip parameter increased both temperature and nanoparticle concentration profiles. Figs. 9-12, it is easy to notice that temperature and nanoparticle concentration profiles decrease with an increase in thermal slip parameter. Figs. 13-16, indicate the effect of concentration slip parameter on temperature and

nanoparticle concentration profiles for $\beta = 0.5\ and\ \infty$, it was observed that there is a slit effect of concentration slip parameter on temperature profile while there is a significant effect on nanoparticle concentration profile. Figs. 17-20,show the enhancement of temperature and nanoparticle concentration and its associated boundary layer thickness with an increase in N_b. Figs. 21-24, represent the effect of Brownian motion parameter on temperature and nanoparticle concentration profiles; it was noticed in figs. 21-22 that increase in N_b leads to increase in temperature profiles for both $\beta = 0.5\ and\ \infty$, while a decrease in nanoparticle concentration profiles was observed with an increase in Nb for both $\beta = 0.5\ and\ \infty$. Figs. 25-28, depict the effect of chemical reaction on nanoparticle concentration profiles when $N_b = 0.1, 0.5$ and it can seem clear from the graphs that increase in chemical reaction depreciates the nanoparticle concentration. Figs. 29-32, display the behaviour of $N_t$on temperature and nanoparticle concentration profiles. It was indicated that an increase in N_t causes increases in both temperature and nanoparticle concentration when $Le = 1\ and\ 5$. Figs. 33-36, are sketched to analyse the influence of N_b on temperature and nanoparticle concentration, and for $Le = 1$, both temperature and nanoparticle concentration decrease as Nb increases, while the increase in $N_b\ for\ Le = 0.5$ enhanced the temperature profile and the reverse was noticed in nanoparticle concentration. It was discovered from figure 37 that the temperature profile is enhanced with an increase in Eckert number. Since the increase in Eckert number leads to an increase in thermal energy which improves the temperature and thermal boundary layer thickness nanofluid.

Figs. 38, it is observed that the rise in Eckert number near the surface cause a decrease in the concentration distribution, while the reverse is indicated away from the surface for$\beta = 0.5$. Figs. 39-40, portray the behaviour of Hartman number H_a on both temperature and nanoparticle concentration for $\beta = 0.5\ and\ \infty$, and it observed that there is an increase in both profiles when there is an increase in Ha. Figs. 41-42 represent the effect of Brownian motion Nb and Hartman number$H_a$on local Nusselt number ($-\theta(0)$) and $-\phi'(0)$, while an increase in N_b causes decreases in local Nusselt number and increase in Nb leads to an increase in $-\phi'(0)$. Figs. 43-44, are plotted to see the behaviour of Brownian motion and Eckert number on both $-\theta(0)$ and$-\phi'(0)$, and it shows graphically that there is a decrease in local Nusselt number and increases in Sherwood number as we increase the value of the Brownian motion parameter.

Table 1: Numerical values of $\left(1 + \frac{1}{\beta}\right) f''(0),\ -\theta', and\ -\phi'(0)\ with\ \lambda, \gamma, \delta, \beta\ for\ N_t = N_b = 0.1, E_c = X = 0.2, Le = 5, and\ P_r = 3$

λ	γ	δ	β	$\left(1 + \frac{1}{\beta}\right) f''(0)$	$-\theta'(0)$	$-\phi'(0)$
0	0.1	0.1	0.5	-1.743300	0.652945	1.37517
1	0.1	0.1	0.5	-0.537442	0.490495	1.05486
3	0.1	0.1	0.5	-0.242811	0.375805	0.9233303
0.1	**0**	0.1	0.5	-1.37247	0.6473183	1.28569
0.1	**0.8**	0.1	0.5	-1.37247	0.425237	1.34874
0.1	**40.1**	0.5		-1.37247	0.168251	1.41875
0.1	0.1	**0**	0.5	-1.37247	0.756331	1.21216
0.1	0.1	**0.5**	0.5	-1.37247	0.281242	1.50214
0.1	0.1	**3**	0.5	-1.37247	-0.0122779	1.53373
0.1	0.1	0.1	**0.3**	-1.367733	0.631137	1.29903
0.1	0.1	0.1	**4**	-0.759598	0.602165	1.27278
0.1	0.1	0.1	∞	-0.914972	0.478581	1.27365

Table 2: Numerical values of $-\theta'(0)$ and $-\phi'(0)$ with N_t, N_b, X, and E_c for $\lambda = \gamma = \delta = 1\ \beta = 0.5, P_r = 3, and\ Le = 5$

N_t	N_b	X	E_c	$-\theta'(0)$	$-\phi'(0)$
0.1	0.1	0.1	0.1	0.698104	1.27562
0.5	0.1	0.1	0.1	0.465085	1.28115
0.9	0.1	0.1	0.1	0.3150585	1.78684
0.1	**0.1**	0.1	0.1	0.698104	1.27562
0.1	**0.3**0.1	0.1	0.499445	1.43289	
0.1	**0.5**	0.1	0.1	0.344926	1.45705
0.1	0.1	**-0.3**	0.1	0.711315	0.564284
0.1	0.1	**0**	0.1	0.700414	1.13417
0.1	0.1	**0.5**	0.1	0.692182	1.71166
0.1	0.1	0.1	**0.1**	0.698104	1.27562
0.1	0.1	0.1	**0.3**	0.448205	1.41412
0.1	0.1	0.1	**0.6**	0.0638096	1.62865

5. CONCLUSIONS

In the present study, the heat and mass transfer in a Cassonnanofluid flow over a stretching sheet with the inclined magnetic field and slip boundary condition is investigated numerically. The concluding facts for the present study after a thorough observation are stated below.

1. Enhancement of both temperature and nanoparticle concentration was observed when there is an increase in thermophoresis parameter Nt.
2. Increase in slip parameter result to decrease in the velocity of the fluid
3. The chemical reaction for $X < 0$ increase the nanoparticle concentration and concentration boundary layer thickness but the reverse is observed for $X > 0$
4. Both temperature and nanoparticle concentration profiles increase with an increase in the magnetic field.

Conflict of interests

On behalf of all authors, the corresponding author states that there is no conflict of interest.

REFERENCES

[1] Choi, S. U. S., "Enhancing Thermal Conductivity of Fluids with Nanoparticle, In D.A. Signer, H.P.Wang Eds.," *Developments and Applications of Non-Newtonian Flows*, **231**, pp.99□105 (1995).

[2] Kandikar and Salman (2003). Convection heat transfer in microchannels using conventional fluids like water and ethylene glycol.Heat Transfer, Vol. 125, pp.151-155.

[3] Hu, C.; Bai, Ml.;Lv, J.; Li, X. (2014). Molecular dynamics investigation of the effect of copper nanoparticle on the solid contact between friction surfaces. Appl. Surf. Sd., 321, 302-309. [CrossRef]

[4] Mustafa, M. and Haynt. T. (2013)."UNSTEADY BOUNDARY LAYER FLOW OF NANOFLUID PAST AN IMPULSIVELY STRETCHING SHEET" Journal of Mechanics, Vol. 29, No, 3.

[5] Clement Kleinstreuer and ZelinXu, (2016). "Mathematical Modeling and Computer Simulations of Nanofluid Flow with Applications to Cooling and Lubrication" Fluids, 1, 16; doi:10.3390/fluidslO200l6.

[6] Alloui, Z., Vasseur, P. and Reggio, M. (2012). "Analytical and numerical study of buoyancy-driven convection in a vertical enclosure filled with nanofluid" Heat Mass Transfer 48:627-639.

[7] Y.M. Xuan, Q. Li, Investigation on convective heat transfer and flow features ofnanofluids, ASME J. Heat Transfer 125 (2003) 151–155.

[8] Bhattaryya, K. (2013). "MHD stagnation-point flow of Casson fluid and heat transfer over a stretching sheet with thermal radiation" Journal of Thermodynamics, Article ID169674.

[9] Khalid, S., Kamal, M.A., Rasheed, U. Farooq, S., Kussain, S. and Waqas, H. (2017). "Buoyancy and the Chemical Reaction Effects on MI-ID Flow of Casson Fluids through a Porous Medium Due to a Porous Shrinking Sheet" .1 Appl. Environ. Biol. Sci., 7(5)154-165.

[10] Mahanthesha, B. and Gireesh, B.J. (2018). "Thermal Marangoni convection in a two-phase flow of dusty Casson fluid" Results in Physics 8: 537—544.

[11] Naveed Ahmed,Umar Khan,Sheikh Irfanullah Khan, SaimaBano Syed TauseefMohyud-Din, (2017). "Effects ofthe magnetic field in squeezing flow of a Casson fluid between parallel plates" Journal of King Saud University — Science 29, 119-125.

[12] Sathies Kumar, P. and Gangadhar, K. (2015). "Effect of chemical reaction on slip flow of MHD Casson

fluid over a stretching sheet with heat and mass transfer" Advances in Applied Science Research, 6(8):205-223.

[13] Samir Kumar Nandy, (2013) "Analytical Solution of MHD Stagnation-Point Flow and Heat Transfer of Casson Fluid over a Stretching Sheet with Partial Slip, Hindawi Publishing Corporation, Article ID 108264, 9 pages.

[14] Waqar A. Khan, J. Richard Culham and 0. Daniel Makinde, (2015)j "Combined Heat and Mass Transfer of Third-Grade Nanofluids over a Convectively-Heated Stretching Permeable Surface" Can. J. Chem. Eng. 93:1880-1888.

[15] Hussain, T., Hayat, T. and Ramzan, M. (2016) "Flow of Cassonnanofluid with viscous dissipation and convective conditions: A mathematical model," J Cent. South Univ.,22: 1132-1140.

[16] Rizwan U Haq, SohailNadeem, ZafarHayat Khan, Toyin Gideon Okedayo, (2014). "Convective heat transfer and MUD effects on Cassonnanofluid flow over a shrinking sheet" Cent. Fur. 3. Phys. 1202), 862-871.

[17] Oyelakin, 1.S., Mondal S. and Sibanda, P. (2016). "Unsteady Cassonnanofluid flow over a stretching sheet with thermal radiation, convective and slip boundary conditions,"Alexandria Engineering Journal, 55, 1025-1035.

[18] Ghosh S-and Mukhopadhyay, S. (2017). "MI-ID slip flow and heat transfer of Cassonnanofluid over an exponentially stretching permeable sheet," International Journal of Automotive and Mechanical Engineering, Vol. 14, No. 4, pp. 4785-4804.

[19] Sidra Aman, SyazwaniMohdZokri, Zulkhibri Ismail, MoMZukiSalleh, Ilyas Khan, (2018). "Effect of MHD and Porosity on Exact Solutions and Flow of a Hybrid CassonNanofluid" Journal of Advanced Research in Fluid Mechanics and Thermal Sciences 44, Issue 1, 13 1-139.

[20]T. Javed and I. ''Mustafa, Slip effects on a mixed convection flow of a third-grade fluid near the orthogonal stagnation point on a vertical surface,'' *Journal of Applied Mechanics and Technical Physics, Vol. 57, No. 3, pp. 527–536, 2016.*

[21] T.Hayata,b, M. IjazKhana, SumairaQayyuma, A.Alsaedib, M. ImranKhanc. '' New thermodynamics of entropy generation minimization with nonlinear thermal radiation and nanomaterials'' Physics Letter A (in press), 2018.